Evidence from high frequency seismic waves for the basalt-eclogite transition in the Pacific slab under northeastern Japan

Wenbo Wu*, Jessica C. E. Irving

Department of Geosciences, Princeton University, Princeton, New Jersey, USA.

Abstract

Seismic multi-pathing effects, attributed to a contrast in seismic attenuation between the back-arc mantle wedge and subducted crust, are detected in central Honshu, northeastern Japan. We observe an initial broadened P-wave which is followed by a delayed higher frequency P-wave signal. Their discrepant frequencies are best explained by attenuation effects: delayed P-wave signals travel in the low-attenuation oceanic crust and therefore contain more high frequency components. The time separation between the initial broadened P-waves and the delayed P-wave signals are affected by the seismic velocity in the subducted oceanic crust. We observe systematic variation in the delay times of the later waves indicating an increase in seismic velocity in the oceanic crust (relative to the mantle wedge) at ∼130-150 km depth. High-frequency seismic simulations incorporating mineral-physics derived models show that a 4% Vp increase due to the blueschist decomposition and a 9% Vp increase associated with the (lawsonite, talc) - eclogite transition replicate the observed delay time variation. The blueschist breakdown may occur at a depth of ∼100 km and the (lawsonite, talc) - eclogite transition might be linked with the reduced seismicity level at depths greater than 150 km. Distinct from traditional guided waves, the multi-pathing effects in this study are mainly controlled by attenuation contrast and therefore may not require the oceanic crust to have low velocity and any special

*Corresponding author

Email address: `wenbow@princeton.edu` (Wenbo Wu)

Submitted to Earth and Planetary Science Letters *May 12, 2018*

decoupling mechanism. The multi-pathing effects offer us another important tool to image subducted oceanic crust below back-arc mantle wedges, especially where guided waves are not observable. In this study, we demonstrate the value of observing and simulating high frequency seismic waves (>20 Hz) in advancing our understanding of subduction zones.

Keywords: seismology, slab dehydration, basalt-eclogite transition, attenuation, multi-pathing, high frequency seismic waves

---

1. Introduction

The upper parts of subducted slabs, including the oceanic crust and the slab's uppermost mantle, are believed to be highly hydrated, with water present in form of hydrous minerals and/or free water. As slabs subduct into higher temperature and pressure environments, a series of metamorphic reactions dehydrate slabs and turn most of the water bound in hydrous mineral into aqueous fluid (*Hacker et al.*, 2003) (Fig. 1). This free water migrates through the mantle wedge and feeds arc volcanic activity, while some amount of mineralogically bound water might remain in the slabs as they descend to their ultimate fate in the deep Earth (*Hacker*, 2008). However, the spatial evolution of water content in slabs during subduction and the specific path of water migration within a mantle wedge are still not fully constrained. Additionally, the genesis of intermediate-focus earthquakes in the subduction context has been proposed to be linked with dehydration embrittlement (*Kirby et al.*, 1996), but other hypotheses, for example plastic instabilities (*Hobbs and Ord*, 1988) and transformational faulting (e.g. *Green and Burnley*, 1989), exist. Thus, a detailed understanding of slab dehydration and metamorphic reactions is critical for understanding both the water cycle within the solid Earth and the physical mechanism for the intermediate-focus seismicity.

Metamorphic reactions in slabs usually lead to changes of seismic properties and therefore could be detected by seismic waves. Thanks to dense, high quality seismic networks such as the High-sensitivity seismograph network (Hi-net, *Okada et al.*, 2004; *Obara et al.*, 2005), the subducting slab beneath Japan is arguably the best imaged on the Earth. Seismic tomography, including velocity and attenuation imaging (for example *Matsubara et al.*, 2008; *Nakajima et al.*, 2013a), has been applied to the slab beneath Japan and provides unprecedented images. However, even under Japan, the seismic tomographic resolution is still limited by ray path coverage and smoothing constraints and is therefore not able to resolve sharp or small scale structure, such as on the scale of oceanic crust which has a thickness of $\sim$7 km. Higher spatial resolution of seismic imaging is critical to address many questions about subduction context. For example, *Nakajima et al.* (2013b) found three earthquake nests at depth of around 150 km in the subducted oceanic crust beneath central Honshu, northeastern Japan (Fig. 2) and indicated that the nests' likely origin is due to dehydration embrittlement caused by eclogitization. Such eclogitization of subducted oceanic crust could only be detected by seismic imaging with high spatial resolution.

Seismic waves trapped in oceanic crust, a form of guided waves, travel along slab interfaces and are therefore sensitive to the oceanic crust's velocity. Observations of guided waves in various slabs, including under Northern Japan, have confirmed the ubiquitous existence of low-velocity (LV) oceanic crust in slabs with old lithosphere (*Abers*, 2000; *Martin et al.*, 2003; *Shiina et al.*, 2017), although the depth range of where the LV crust is present may vary among different slabs. However, *Furumura and Kennett* (2005) proposed an alternative model of elongated heterogeneities parallel to the plate margin to explain dispersed guided waves, in which an LV oceanic crust is not necessary. In this study, we find multi-pathing phenomena from intermediate-focus earthquakes beneath central Honshu, northeastern Japan and attribute it to the attenuation and velocity differences between mantle wedge and oceanic crust. Distinct from traditional guided waves, the multi-pathing effects in our study are mainly controlled by the remarkably different attenuations present, and therefore not limited to the scenario of LV oceanic crust. Using SPECFEM2D (*Komatitsch and Tromp*, 1999), we compute the sensitivity kernels of the direct P-waves and the delayed high frequency signals, which clearly illustrate their different travel

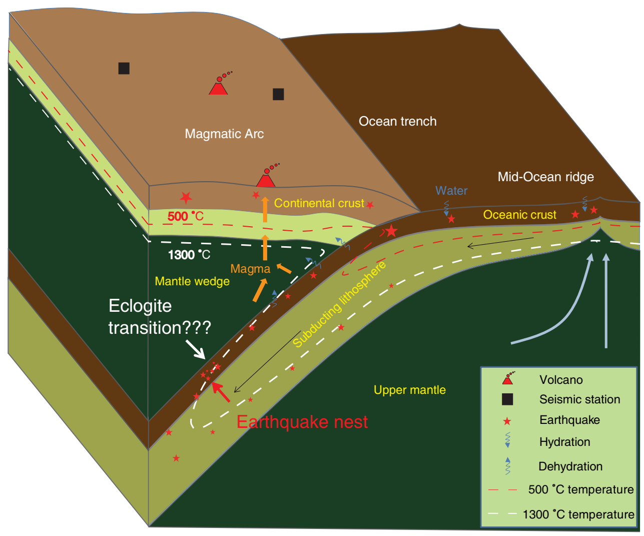

Figure 1: Cartoon showing the tectonic setting of a subducting slab (not to scale). The earthquake nest may be related to the eclogite transition.

paths and explain the multi-pathing effects well. After testing different crust models, comparison of the synthetic seismograms with observations indicates a likely velocity increase in the oceanic crust at a depth of ∼138 km.

2. Data and observations

Here we use high frequency seismic waves, recorded at Hi-net stations, generated by intermediate-focus earthquakes to investigate the structure of the oceanic crust.

2.1. Hi-net seismograms

The Hi-net stations contain borehole seismometers with a natural frequency of 1 Hz and high sensitivity in the high frequency range (their sampling frequency is 100 Hz, *Okada et al.*, 2004; *Obara et al.*, 2005). Fig. 3 shows seismograms from five Hi-net stations corresponding to an earthquake at a depth of 155 km. After removing the instrument responses, we identify the onsets of the direct P-waves, on which the seismograms are aligned in Fig. 3a. It is

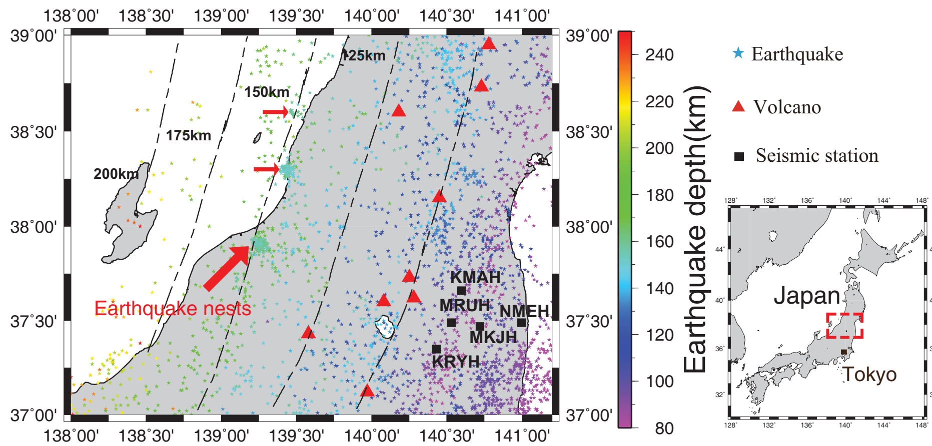

Figure 2: Map of central Honshu, northeastern Japan (left figure) and location of this region (red box, right). Colored stars represent earthquakes between 2004-2013 (catalog from Japan Meteorological Agency). The black dashed lines are contours corresponding to the estimated geometry of the top interface of the subducted Pacific plate (*Zhao et al.*, 1997; *Nakajima et al.*, 2013b). The three red arrows point out the concentrated seismic clusters. All of the three clusters, or earthquake nests, are located below the top interface of the slab which has a depth of ∼150 km.

difficult to clearly identify the onset at NMEH due to the low Signal to Noise Ratio (SNR). While there are more Hi-net stations in this region, they are not used here due to either low SNR or raypaths which deviate from the up-dip direction. By analyzing the waveforms, we find apparent multi-pathing effects: multiple signals traveling with different raypaths. In the first few seconds after the onsets, there are two distinct P-wave signals with different travel times and frequency contents. A broad direct P-wave is followed by a signal containing high frequency components. After applying a high frequency filter (>20 Hz), the delayed signals are clearer (Fig. 3b).

We collect data for 312 earthquakes in the period 2004-2013 from the JMA earthquake catalog. The horizontal locations of the 312 events (Fig. 4a) are within 20 km of the up-dip projected line. Thanks to the ultra-dense network and seismically quiet environments of the Hi-net stations, Japan has an excellent seismic detection capability that provides us with rich data from small

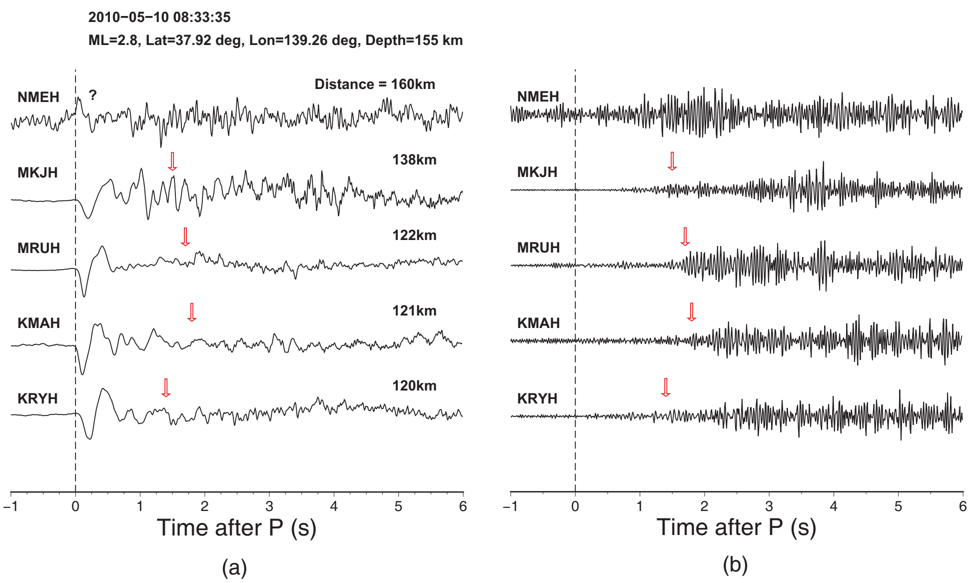

Figure 3: Seismograms recorded at five Hi-net stations (shown as black squares in Fig. 2) for event #100510. The hypocenter of this earthquake is within the earthquake nest marked by the large red arrow in Fig. 2. (a) Raw seismograms aligned on the identified onsets of P-waves. The red arrows mark the delayed high frequency signals. (b) Seismograms after applying a high frequency filter (>20 Hz). The time zero in (a) and (b) is the onset of direct P-wave.

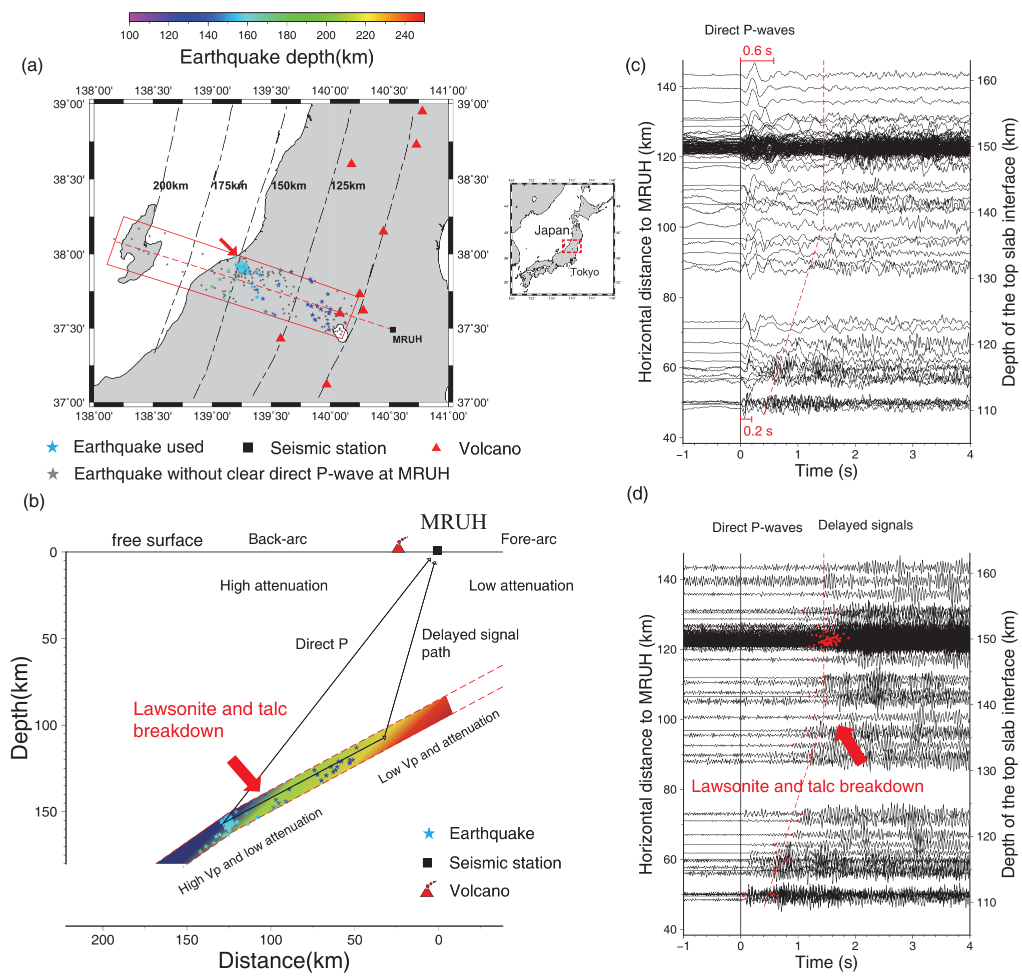

Figure 4: Map, depth cross section and seismic data. (a) Map of earthquakes. The red arrow points to the earthquake nest. Stars represent the total 312 earthquakes and the colored stars are earthquakes with clear seismograms at station MRUH. (b) Schematic figure illustrating the ray paths of the direct P-wave and delayed signal. The upper red dashed line shows the estimated geometry of the top interface of the subducted Pacific plate and the lower one illustrates the oceanic Moho discontinuity. In our interpretation of attenuation controlled multi-pathing effects, the delayed signals first travel in the oceanic crust then to the seismic station. (c) Distance profile of seismograms after filtering (high pass >1 Hz). (d) Distance profile of seismograms after high frequency filtering (>20 Hz). The red dots indicate the arrivals of the delayed signals. The black lines in (c) and (d) represent the onsets of direct P-waves, while the red lines show the delayed signal arriving. The seismograms are aligned on the onsets of direct P-waves and plotted with normalized amplitude in both (c) and (d).

earthquakes. These 312 earthquakes used have a JMA magnitude range of M0.8-M3.7 and 172 of them have M$\leq$2.0. The ultra-dense coverage also results in accurate earthquake locations. For this region, clear double belts of intermediate-focus seismicity, the Wadati-Benioff zone, have been imaged and the upper plane seismic belt is mainly concentrated in the subducting oceanic crust (*Kita et al.*, 2006). Here, we focus on the structure of the oceanic crust, so only the earthquakes in the 7 km directly below the top slab interface are used (Fig. 4b). Among the five records in Fig. 3, MRUH has the best SNR (for both raw data and the delayed signals) and is closest to the slab up-dip projected line (red dashed line in Fig. 4a), which crosses the earthquake nest. Thus, we choose this typical station with optimal geometry to investigate the multi-pathing effects. Finally, we get 98 good records from MRUH, in which the onsets of the direct P-waves are sufficiently clear to be observed.

2.2. Data interpretation

After 1 Hz high pass filtering (Fig. 4c), all the 98 seismograms have SNR>2.0 and 88 of them have SNR>3.0. The direct P-waves are increasingly broadened with increasing horizontal distance. This feature is also visible in the raw data (Fig. S1a). The widths of direct P-waves (the first arriving phases) generally increase with the horizontal distance to MRUH from 0.1-0.2 seconds to 0.4-0.6 seconds in Fig. 4c (waveforms from the zoomed-in earthquake nest are shown in Fig. S2). Following the direct P-waves, the high frequency signals are weak but still visible across all the records (immediately after the red dashed lines in Fig. 4c) and become clearer in higher frequency bands of 7-16 Hz and 16-25 Hz (Fig. S1c and d). After applying a high frequency filter (>20 Hz), the delayed signals dominate the seismograms and are much stronger than the direct P-waves on most records, except the closest few records, where the direct P-waves also contain high frequencies. We pick the arrivals of the delayed signals (red dots in Fig. 4d) and use the red dashed line to roughly outline their variation as a function of depth and/or distance. Relative to the direct P-wave, the arrival delays of the high frequency signals first increase and then become constant with the horizontal distances between earthquakes and the station (Fig. 4d). The change happens at a horizontal distance to MRUH of roughly 101 km, which is mapped to a depth of 138 km on the slab-top interface. Of course, some data significantly deviate from the red dashed lines. That is at least partly due to the difficulty of identifying arrivals of the high frequency extended wave train in the presence of noise. For example, the picked arrivals show a large variability among the earthquakes from the nest, but the delayed signal assemblage, as a whole, has high waveform similarity (Fig. S2).

As a typical example of seismic multi-pathing in subduction contexts, observations of guided waves are widespread and have been used to constrain properties of subducted oceanic crust. However, guided waves alone cannot explain our data. First, guided waves are usually reported as dispersed body waves with dominant frequency less than 16 Hz (e.g. *Abers*, 2000; *Martin et al.*, 2003; *Takemura et al.*, 2015a,b; *Shiina et al.*, 2017), but our data show two temporally well-separated signals with distinct frequency contents. Furthermore, station MRUH is further west of the slab updip extension point on the free surface (Figs. 4a,b), where guided waves can be decoupled from oceanic crust and are therefore most likely to be observed.

We propose another mechanism, to which attenuation contributes, to explain the multi-pathing phenomena here. As Fig. 4b shows, the direct P-waves mainly propagate in the mantle wedge while the delayed signals travel within the oceanic crust and then are deflected into the fore-arc mantle. Thus, the different frequency contents of the direct P-waves and delayed signals can be best explained by attenuation effects. High attenuation of the back-arc mantle wedge, mainly due to partial melting or premelting, is present in various attenuation tomography models (*Nakajima et al.*, 2013a; *Liu et al.*, 2014), so high frequency content of the direct P-waves is heavily attenuated. Thus, the broadened direct P-waves in Fig. 4c can be best explained by attenuation, the effect of which is proportional to the distance traveled. In contrast, cold subducted slabs feature low attenuation, so high frequency waves traveling in the oceanic crust can survive and emerge in the delayed signals. Although part of the ray paths of the delayed signals is also located in the fore-arc mantle and crust, this length is shorter than the direct P-waves. Additionally, the fore-arc mantle and crust have lower attenuation than the back-arc (*Nakajima et al.*, 2013a; *Liu et al.*, 2014) (Fig. 4b) due to its colder thermal environment.

3. Mineralogical and seismological simulations

In the following two subsections, we describe numerical modeling conducted to explain the attenuation controlled multi-pathing effects and then use the delayed signals to constrain the structure of the oceanic crust. In subsection 3.1, we briefly summarize some previous research on phase transitions and carry out calculations of the phase assemblages of oceanic crust. We also summarize some previous studies of P-T paths and seismic velocity beneath northeastern Japan, which are used in the next subsection. In subsection 3.2, the multi-pathing effects are successfully duplicated by numerical simulations of wave propagation and Vp (P-wave velocity) in the oceanic crust is investigated by comparing synthetic seismograms to data.

3.1. Phase transitions, P-T paths and seismic velocity of the subducted oceanic crust beneath northeastern Japan

Mineralogy predicts that subducted oceanic crust undergoes several phase transitions and concomitant dehydration, resulting in seismic velocity increases (e.g. *Hacker et al.*, 2003). However, where and how those phase transitions develop in various subduction zones is not fully understood due to the large uncertainties of phase diagrams and thermal environments. Experiments regarding phase transitions in oceanic crust rocks are reported, but they only sample a limited number of bulk compositions and pressure-temperature (P-T) conditions.

We calculate the mineral assemblages which may be present as crust is subducted. We make the simplifying assumption that the oceanic crust is composed of basalt and use Perple_X (*Connolly*, 2005), a Gibbs free energy minimization method, to calculate the mineral assemblages at different P-T conditions. Following *Hacker* (2008), we further assume water saturation of the basalt and then calculate the water content bound with the hydrous minerals (Fig. 5a), which is an agent of phase transition. We note that the not fully-constrained thermodynamic parameters used in Perple_X could introduce some uncertainties in the estimated water content in Fig. 5a, but they are not expected to significantly change the general pattern predicted at relevant conditions. We repeat this calculation for a bulk composition of gabbro, which shows the same general pattern as basalt (Fig. S3). At $P > 3$ GPa, the P-T boundaries of most phase transitions from hydrous to nominally anhydrous minerals roughly follow isothermal curves (Fig. 5a). The increased temperature of subducted oceanic crust due to heating from the mantle-wedge, causes phase transitions and concomitant dehydration. The blueschist - eclogite and (lawsonite, talc) - eclogite transitions release a large volume of water (Fig. 5a), which may facilitate the intermediate-focus seismicity beneath northeastern Japan (*Kita et al.*, 2006; *Shiina et al.*, 2013; *Nakajima et al.*, 2013b).

We know those transitions must occur as subducting slabs heat up, but the simulated P-T paths of slabs vary dramatically between different studies due to different model setups and rock properties used. For example, the P-T paths for our study region produced by *Iwamori* (2007) and *Syracuse et al.* (2010) show large differences away from their intersection at ~3 GPa (Fig. 5a). In the chemically interacting system composed of the mantle-wedge and slab, many less well understood factors, such viscosity and the depth of coupling-decoupling between slab and overlying mantle-wedge, affect thermal exchange and introduce uncertainties in P-T estimations.

Shiina et al. (2013) found an abrupt Vp increase in the subducted oceanic crust at a depth of ~100 km (Fig. 5b), using P-to-S converted waves. Another Vp increase seems to happen at ~130-150 km depth. The depths of those two Vp increases are spatially correlated with, and therefore might be physically linked with, the intermediate-focus seismicity (*Kita et al.*, 2006). Slab P-T paths cross the line of blueschist - eclogite transition at a pressure of ~3 GPa

(Fig. 5a), close to ∼100 km depth. As pressure increases, the basalt undergoes the (lawsonite, talc) - eclogite transition, but the P-T model of *Iwamori* (2007) predicts that the slab is a much colder environment, leading to a greater depth of this phase transition, than that modeled by *Syracuse et al.* (2010).

In summary, two major phase transitions occur in the subducted oceanic crust beneath northeastern Japan. The shallower one associated with the blueschist breakdown occurs at a depth of ∼100 km, below which water migrates up to hydrate and form the back-arc mantle wedge. In our study region, the ∼100 km depth slab geometry contour projected on the free surface matches the location of the volcanic arc (Fig. 4a). Thus, the ∼100 km depth contour and the volcanic arc might together outline an almost vertical boundary between fore-arc mantle and back-arc mantle (Fig. 4b). As we show, the delayed high frequency signals travel within the oceanic crust and then are deflected into the fore-arc mantle. The deflection is expected to occur at the back-arc to fore-arc transition, a depth of ∼100 km (Fig. 4b). This prediction is consistent with the data shown in Fig. 4d, where the arrivals of direct P-waves and the delayed high frequency signals would, if extrapolated, intersect at a depth ∼100 km. The (lawsonite, talc) - eclogite transition occurs at a greater depth, where the estimations of P-T conditions have larger uncertainty. Based on the Vp imaging of *Shiina et al.* (2013), this transition occurs at ∼130-150 km depth. In the following subsection, we incorporate this Vp imaging result into numerical modeling to explain the seismic data.

3.2. SPECFEM2D simulations

In this subsection, we use the Spectral Element Method (SEM) software package SPECFEM2D (*Komatitsch and Tromp*, 1999) to simulate wave propagation in the subduction zone and explain the multi-pathing effects present.

SEM combines advantages of the spectral method and the finite element method and is able to accurately deal with many types of seismic complexities, such as irregular internal discontinuities, attenuation and anisotropy (*Komatitsch and Vilotte*, 1998; *Komatitsch and Tromp*, 1999). Currently, there

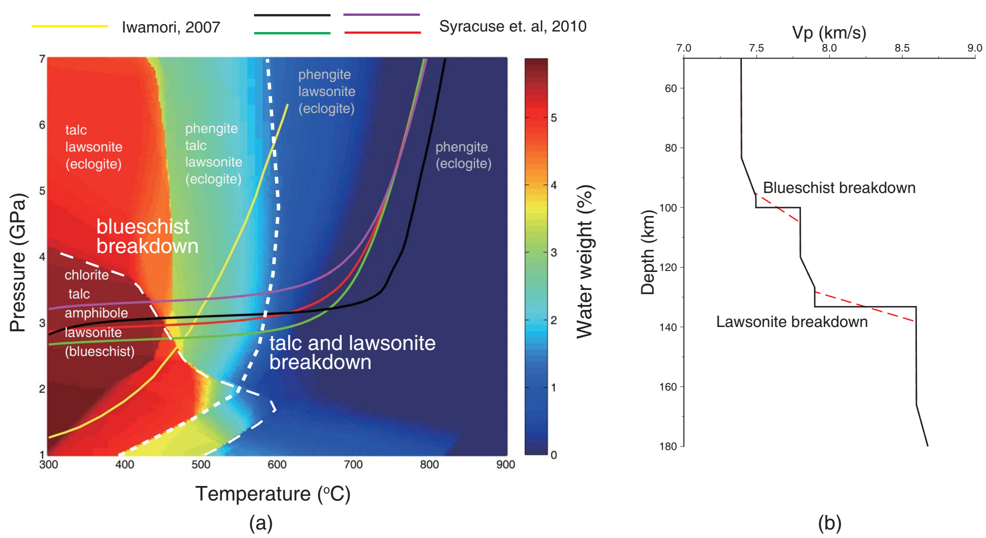

Figure 5: Phase map and Vp as a function of depth. (a) Phase diagram of basalt saturated with H_2O calculated with Perple_X. The bulk composition of basalt is from *Hacker* (2008). The yellow and other colored lines correspond to P-T path models by *Iwamori* (2007) (his North East Japan profile) and *Syracuse et al.* (2010) (their central Honshu profiles) respectively. The white dashed lines outline the approximate boundaries of metamorphic faces and mineral phase transitions. (b) Adapted and original Vp models of the oceanic crust beneath northeastern Japan from *Shiina et al.* (2013), based on mineral physics and thermal estimates (*Hacker et al.*, 2003). The red dashed lines represent 10 km wide velocity transitions implemented here.

are three versions of the SPECFEM software packages. Relevant here are SPECFEM2D, which solves problems of wave propagation in a 2D space domain, and SPECFEM3D_Cartesian, which solves 3D problems at a local or regional scale. SPECFEM3D_Cartesian has been used to compute wave propagation in 3D models of subduction zone (e.g. *Chen et al.*, 2007). However, in contrast to that study, the delayed signals in our data contain high frequencies (>20 Hz), so 3D simulations of wave propagation are too computationally expensive. We simplify the problem to 2D and adopt SPECFEM2D (*Komatitsch and Tromp*, 1999) to simulate wave propagation. Because we restrict the source-receiver geometry to be mainly in the up-dip direction, a 2D model is a reasonable simplification for the purpose of this study. Additionally, comparison between 2D and 3D numerical simulation of wave propagation has been reported in previous studies of high frequency trapped waves in oceanic lithosphere (*Takemura et al.*, 2015a; *Kennett and Furumura*, 2008) and shows no significant differences. We use an explosion source in the SPECFEM2D simulations, which gives rise to isotropically radiated P-waves. Although the radiation patterns of earthquakes are non-isotropic, this is a reasonable approximation for high frequency seismic waves (*Kobayashi et al.*, 2015).

3.2.1. Simulation of attenuation controlled multi-pathing

In subsection 3.1, we discuss the blueschist breakdown starting at a depth of ∼100 km and its link with the formation of back-arc mantle wedge. This link is also supported by attenuation tomography (e.g. *Nakajima et al.*, 2013a; *Liu et al.*, 2014). Seismic attenuation is quantitatively described by the reciprocal quality factor Q^{-1}. In general, back-arc mantle wedges are often partial melt- and water-rich and exhibit high attenuation (low Q) while fore-arc mantles have relatively low attenuation (high Q) due to their low temperatures. A significant attenuation contrast across the volcanic arc, matching the ∼100 km depth contour of the slab geometry, has been reported below northeastern Japan (*Nakajima et al.*, 2013a; *Liu et al.*, 2014). Compared to the back-arc mantle, the old subducted slab, composed of oceanic crust and underlying slab mantle, usually has cold temperature and low attenuation. For example, *Shiina et al.* (2018) use the spectral ratio technique and find Qp of $\sim$ 670 at depths of 50-250 km in the Pacific slab beneath northeastern Japan. Although their data is primarily sensitive to the slab mantle, some paired ray paths seem to sample and therefore reflect the attenuation of subducted oceanic crust. Another line of evidence for low attenuation of subducted oceanic crust is from the study of guided waves by *Garth and Rietbrock* (2014a). Here, we combine these results to form a simple Qp and then conduct SPECFEM2D simulations to demonstrate the attenuation controlled multi-pathing effects (Fig. 6).

We take a slice along the up-dip direction of the slab with dimensions of 241 km (horizontal) $\times$ 272 km (vertical) to create a 2D model. We start by considering only the effects of attenuation. In order to investigate the effects of attenuation, we make the seismic velocity as simple as possible with a uniform Vp = 8 km/s, Vs (S-wave velocity) = 4.5 km/s and density = 3.4 g/cm^3 at infinite frequency. Because of the physical dispersion associated with attenuation, seismic velocity at a finite frequency is a little lower than infinite frequency. We use a simple block-composed Qp model (gray background in Figs. 6c,d) based on some sensible estimations of Qp. We set an extremely low Qp of $\sim$70 in the back-arc mantle and a high Qp of $\sim$630 in the fore-arc mantle. Considering the low temperature in the slab, we assume a Qp of 632 (corresponding to a 2D Qμ = 200) in the oceanic crust and set an even higher Qp of 743 in the slab mantle. A moderate Qp of 379 is introduced in the continental crust. We note that this Qp model reflects many features of attenuation in a real subduction context, but the absolute values of Qp used might have great uncertainty. For example, the Qp$\simeq$70 in the back-arc mantle is lower than previously reported Qp in our study region (e.g. *Nakajima et al.*, 2013a; *Liu et al.*, 2014), although extremely low Qp has been reported in other slabs, e.g. Qp$\sim$56-70 beneath the volcanic arc in the Mariana subduction (*Pozgay et al.*, 2009). Additionally, attenuation tomography usually has large uncertainties (see, for example, significantly different Qp for our study region revealed in Line E of Fig. 10 in *Nakajima et al.*, 2013a and profile E-E' of Fig. 10 in *Liu et al.*, 2014). Thus, we just use Qp$\simeq$70 in the back-arc mantle here and test different Qp models in the next subsection (3.2.2), where a more realistic Vp model is also used.

The model is meshed with 3000 $\times$ 3000 elements to resolve 20 Hz seismic waves. We use an explosion source at a depth of 150 km and specify a Ricker wavelet of source time function with a duration of 0.05 seconds. The receiver is buried at a depth of 103 m, the same as the borehole station MRUH. The time step is 0.0009 seconds and we use 37000 steps, giving a seismogram duration of 33.3 seconds. The simulation result shows clear multi-pathing effects (Figs. 6a,b). There is a clear first arrival of direct P-wave in the raw synthetic, followed by a much weaker signal arriving at the time of around 25.5 seconds (Fig. 6a). Because of strong attenuation the direct P-wave is broadened compared to the input source duration. After applying a high frequency filter (>20 Hz), the delayed signal becomes clear (Fig. 6b).

Thanks to the sophisticated technique of sensitivity kernels implemented in SPECFEM2D (*Tromp et al.*, 2005), we can compute the multiple travel paths in a quantitative way. An advantage of this technique is that we can compute sensitivity kernels for waveforms in a given time window and particular frequency band (*Luo et al.*, 2013). The computation of sensitivity kernels includes an extra process of interacting two wavefields and therefore is more computationally expensive than forward modeling, especially for inelastic media. In contrast to ray theory, which assumes an infinite frequency, the sensitivity kernels provide an area of high travel time sensitivities, instead of an infinitely narrow ray. The travel time sensitivity kernels of the direct P-wave reveal a relatively simple travel path, directly from the source to the receiver (Fig. 6c). Because the delayed signal is weak in the raw synthetic and strong at high frequency, we take the delayed signal in the filtered seismogram (enclosed by the black dashed line box in Fig. 6b) as the input source time function of an adjoint source and compute its travel time sensitivity kernels (as in *Luo et al.*, 2013). Its Vp sensitivity kernels are more complex than the direct P-wave. The first section of the high frequency sensitivity kernels is mainly limited to the oceanic crust. The rest of the kernels shows that the wave is deflected into the fore-arc mantle at a depth of ~100 km (Fig. 6d). The width of the innermost high sensitivity kernel (red area) is much narrower than the direct P-wave due to its high frequency content. These sensitivity kernels are consistent with our interpretation of multi-pathing effects (Fig. 4b).

In previously reported guided waves (e.g. *Abers*, 2000; *Martin et al.*, 2003; *Shiina et al.*, 2017), an LV oceanic crust is required to trap seismic waves. Here, the oceanic crust has either the same Vp (at infinite frequency) as the mantle wedge or even higher Vp (at finite frequency). Thus, the multi-pathing phenomenon is purely produced by the attenuation contrast, without LV oceanic crust. Of course, more complex seismic velocity structures in a real subduction context could affect the amplitudes of the direct and delayed signals. For example, the existence of LV oceanic crust can trap more seismic energy within it and therefore further increase the amplitude of the delayed signal in Fig. 6b.

3.2.2. The impact of dehydration of the subducted oceanic crust on the high frequency signal delay

We now implement a more realistic velocity model (Fig. 7a) to explain the seismic data. We use LITHO1.0 (*Pasyanos et al.*, 2014) to represent the crust structure and the local 1D reference model JMA2001 (*Ueno et al.*, 2002) for the mantle-wedge and mantle below the slab. While JMA2001 may not be fully representative of the mantle below the slab, this would not affect our conclusion due to the low sensitivity of the direct P-waves and delayed signals to the sub-slab mantle. The slab mantle is represented by an angled layer with a velocity 2% greater than the ambient mantle of JMA2001. We introduce a uniform 2% high velocity anomaly in the slab mantle due to its cold temperature, although the real slab mantle may have more complex structure. For example, the uppermost slab mantle might be also greatly hydrated (*Garth and Rietbrock*, 2014b) and therefore has much lower average velocity than that in the lower slab mantle. However, the detailed hydration of the uppermost slab mantle is still an open question and we use a uniform 2% high velocity anomaly for simplicity. We use the Vp depth profile in Fig. 5b (*Hacker et al.*, 2003; *Shiina*

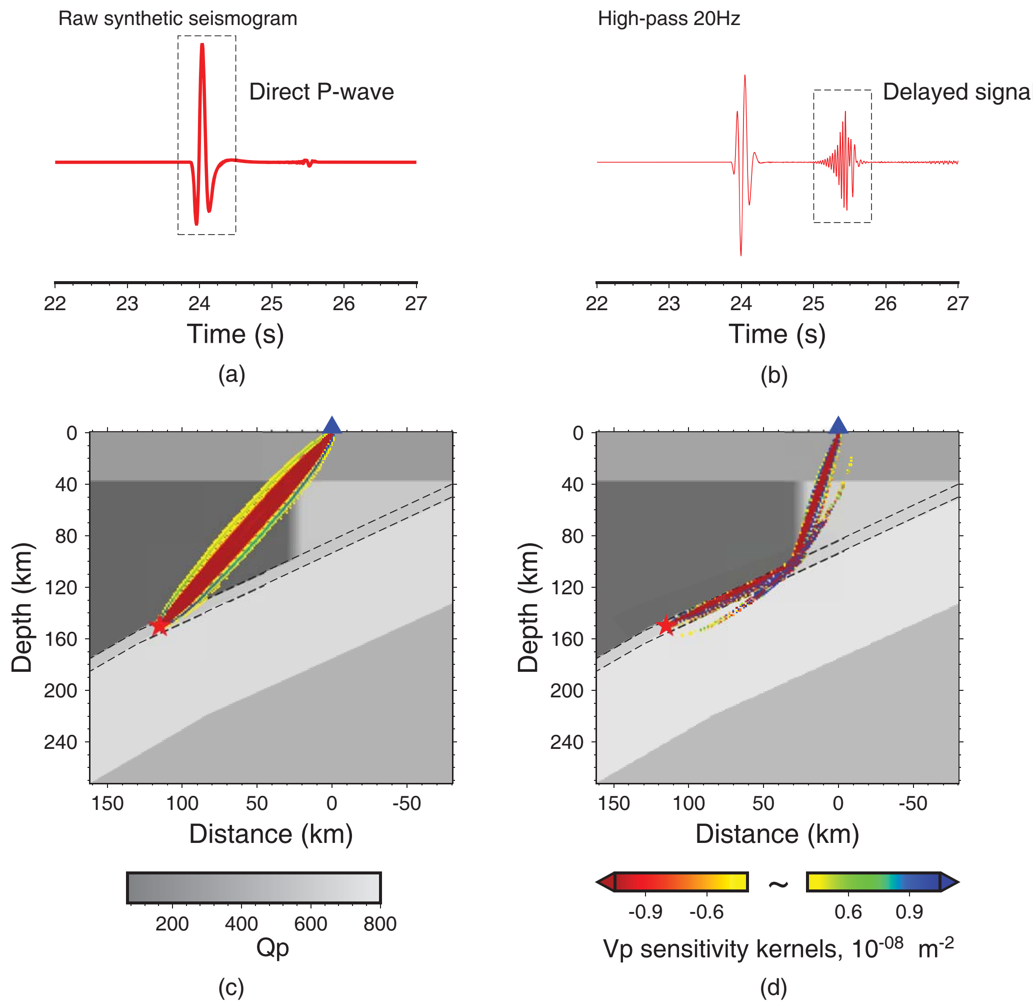

Figure 6: Multi-pathing effects due to the attenuation contrast between back-arc mantle and oceanic crust. (a) Raw velocity synthetic seismograms. (b) Velocity synthetic seismograms after high frequency filtering (>20 Hz). (c) Vp travel time sensitivity kernels for the direct P-wave in the time window enclosed by the black dashed line box in (a). In this model, the subducted oceanic crust is indicated by the two black dashed lines. The gray background represents the Qp model. The seismic velocity model comprises a uniform Vp = 8 km/s and Vs = 4.5 km/s (at infinite frequency). The red star shows the source location and the blue triangle is the receiver. (d) Vp travel time sensitivity kernels for the delayed high frequency signal in the time window of the black dashed line box in (b). The high Vp sensitivity kernels are mainly concentrated within the oceanic crust and then deflected to the fore-arc mantle at a depth of ∼100 km.

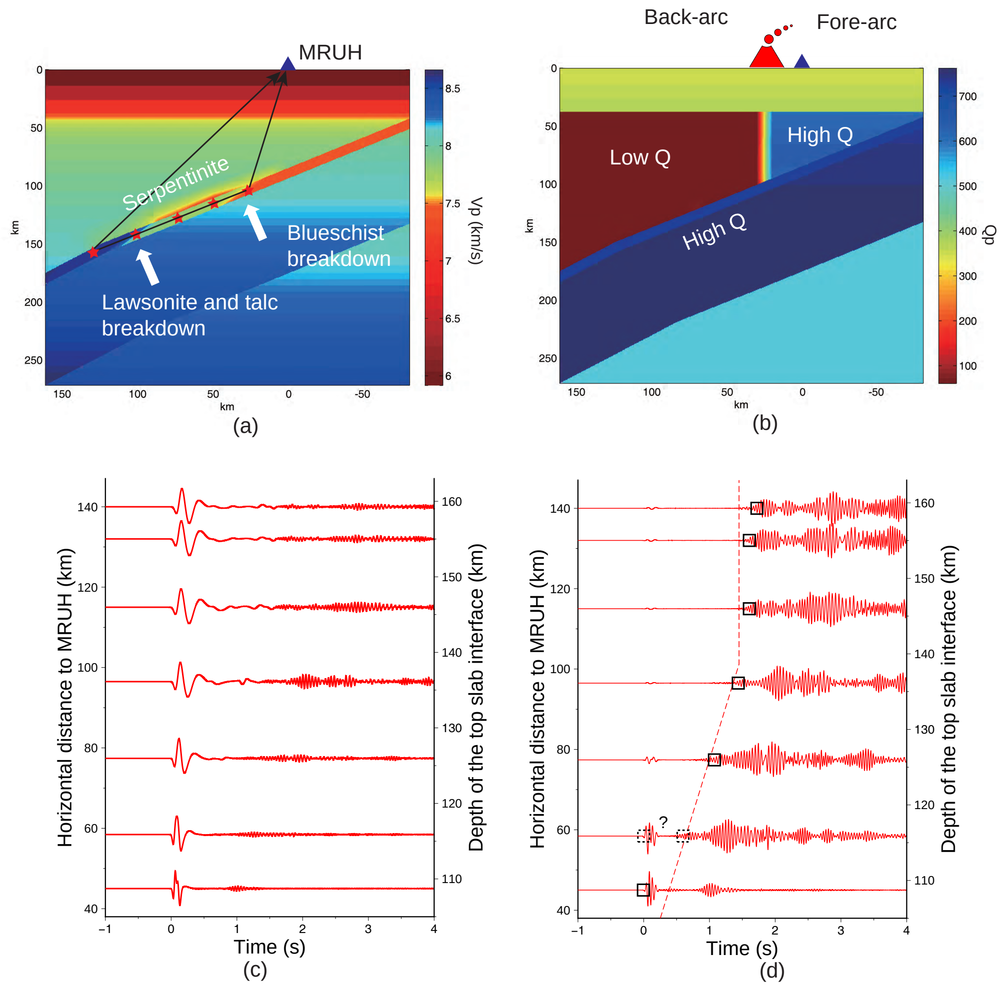

Figure 7: Vp and Qp models and synthetics. (a) Vp model. The blue triangle shows the location of station MRUH and red starts represent the simulated (explosion) sources. The black lines represent the cartoon raypaths of the direct P-waves and delayed signals. (b) Quality factor (Qp) model. The volcanic arc separates the mantle wedge into two parts with significantly different Q values. (c) Distance profile of synthetics after applying a high pass filter (>1 Hz). (d) Synthetics after applying a high pass filter (>20 Hz). The black squares represent the arrivals of the delayed signals. The question mark indicates an ambiguous arrival. The red dashed line is exactly the same as in Figs. 4c,d. The seismograms are aligned on the onsets of the direct P-waves and plotted with normalized amplitude in both (c) and (d).

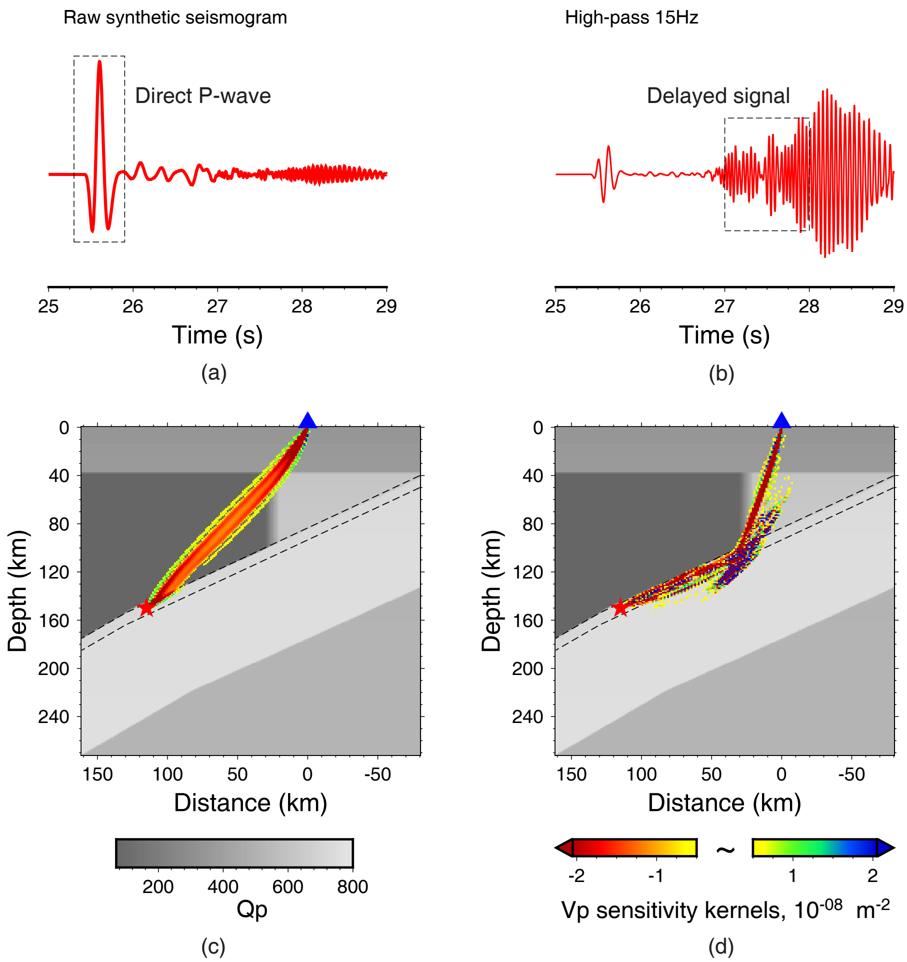

Figure 8: Vp sensitivity kernels of multi-pathing effects displayed in Fig. 7. The velocity model used here is the same as in Fig. 7. (a) Raw velocity synthetic. (b) Velocity synthetic after high frequency filtering (>15 Hz). (c) Vp travel time sensitivity kernels for the direct P-wave (black dashed line box in (a)). The subducted oceanic crust is indicated by the two black dashed lines. The gray background represents the Qp model. The red star shows the source location and the blue triangle is the receiver. (d) Vp travel time sensitivity kernels for the delayed high frequency signal (black dashed line box in (b)).

et al., 2013) for the oceanic crust, modifying the two sharp discontinuities at 100 km and 133 km to occur over a thickness of 10 km to better represent the gradual phase transition. Receiver function results reveal a low velocity zone immediately above the oceanic crust (*Kawakatsu and Watada*, 2007), so we introduce a low velocity layer. The corresponding Vs model is displayed in Fig. S4. The model is meshed with 4000 $\times$4000 elements leading to a mesh grid spacing of $\sim$60m, which is sufficiently fine to resolve 20 Hz seismic waves. We implement the same Qμ model as in subsection 3.2.1. However, the Vp/Vs ratios here are slightly different, causing small differences in the Qp model, because $Qp = Q\mu \times (Vp/Vs)^2$.

We simulate sources in the center of the subducted oceanic crust at horizontal distances from MRUH of 40-140 km. Although a duration of 0.05 seconds is specified for the sources, the duration of the direct P-wave arrivals are longer than 0.05 seconds due to attenuation (Fig. 7c). Specifically, they increase with the horizontal distance, from $\sim$0.2 seconds to $\sim$0.6 seconds; this duplicates the data (Fig. 4c) well. The delayed signals become clearer in a higher frequency band (Fig. S5), as in the data (Fig. S1). After high frequency filtering, the delayed signals have much stronger energy than the direct P-waves. We pick the arrivals of the delayed signals (black squares in Fig. 7d), which show a similar trend to the data (red dashed lines in Figs. 7d and 4d). Similar to the data, the direct P-waves at the closest horizontal distances to MRUH also contain high frequencies; this causes ambiguity in picking the delayed signal (the black dashed squares in Fig. 7d).

In these attenuation controlled multi-pathing effects, the amplitudes of direct P-waves and delayed signals significantly depend on the Qp model. A weak attenuation contrast between the back-arc mantle and oceanic crust would fail to duplicate the multi-pathing effects (demonstrated in Fig. S6). In the SPECFEM2D simulations, we introduce an extremely low Qp $\simeq$ 70 in the back-arc mantle, lower than the Qp estimated by attenuation tomography for our study region (e.g. *Nakajima et al.*, 2013a; *Liu et al.*, 2014). However, attenuation tomography usually has large uncertainty. We test a Qp model, in which only a portion of back-arc mantle near the volcanic arc has a Qp of ∼70 and the rest has a relatively high Qp≃150 (Fig. S7). This model also successfully duplicates the multi-pathing effects, showing that the back-arc mantle does not necessarily have a uniformly extremely low Qp.

To assess the travel paths, we again compute the sensitivity kernels. Because simulation of an adjoint wavefield is more computationally expensive than forward modeling, we have to reduce the number of elements to 3000 × 3000, which is able to resolve 15 Hz waves for the current velocity model (Fig. 7a). Although the number of elements used here is the same as in subsection 3.2.1, the minimum seismic velocity is lower and the maximum resolved frequency is consequently reduced. Comparing to the simulations in Fig. 6, using a more realistic velocity model does not significantly change the travel paths of the direct P-wave and the delayed high frequency signal. The travel path of direct P-wave is similar to that in Fig. 6c, although slightly altered by some complex seismic structures, such as the Moho discontinuity. The high frequency signal still travels within the oceanic crust and is then deflected to the back-arc mantle at a depth of ∼100 km (Fig. 8d), but its detailed pattern is more complex than that shown in Fig. 6d. We note that the delayed signals in our study are P-to-P converted waves and that P-to-S converted phases in our study region have been reported (*Shiina et al.*, 2013), but arrive much later.

The sensitivity kernels prove that the high frequency signal is sensitive to the velocity of subducted oceanic crust. Thus, it can be used to investigate the transitions of blueschist - eclogite and (lawsonite and talc) - eclogite proposed by *Shiina et al.* (2013) (Fig. 5b). We test two additional Vp models of the oceanic crust (full model details are contained in the supplementary material; velocity models are shown in Fig. 9a). In the first test, we retain the Vp increase due to the blueschist breakdown, but remove the lawsonite and talc breakdown. This model also generates multi-pathing effects (Fig. S8) and the arrivals of delayed signals (green triangles in Fig. 9b) fit the data well at the horizontal distances to MRUH less than 120 km. However, the arrivals at horizontal distances to MRUH greater than 120 km are >0.6 seconds later than in the data due to the lack of lawsonite and talc breakdown.

In another test, we remove both of the Vp increases associated with the transitions in Fig. 5b and repeat the simulations. This Vp model corresponds to a uniform LV oceanic crust and produces clear delayed signals (Fig. S10). However, the arrivals of delayed signals (blue diamonds in Fig. 9b) are even later than the previous model and therefore cannot fit the data (red circles in Fig. 9b). Thus, our study supports the occurrences of both the blueschist - eclogite and (lawsonite and talc) - eclogite transitions in the oceanic crust.

As we show in subsection 3.2.1, LV oceanic crust is not necessary in these attenuation controlled multi-pathing effects. For example, there are clear delayed signals from the two sources with depth>150 km in Fig. 8d, although the oceanic crust there has a higher Vp than the overlying mantle wedge and underlying slab mantle (Fig. 8a). Furthermore, at least two special mechanisms have been proposed to make guided waves leak out from the oceanic crust. The first is geometrical bending of slab (*Martin et al.*, 2003), and the second is the equalization of seismic velocity between oceanic and continental crust (*Martin et al.*, 2005). For our scenario, these two special mechanisms might not be necessary, because the multi-pathing effects naturally occur, as long as the marked attenuation contrast is present (Figs. 6-8 and S8-S10). The multi-pathing effects in our study greatly depend on the depths of earthquakes. These effects become stronger, in terms of greater amplitude contrast and/or larger arrival time separations between direct P-waves and delayed signals at high frequency, as the depth of earthquake increases (Fig. 4d and 7d). They provide an important tool to investigate the structure of subducted oceanic crust below the back-arc mantle wedge. However, our data do not sample the oceanic crust at depths shallower than $\sim$100 km (Fig. 7a and 8d), where guided waves can be used to image LV oceanic crust (e.g. *Shiina et al.*, 2017).

In summary, our interpretation of the observed signals being caused by the multi-pathing effects is confirmed by the sensitivity kernels. We use a relatively simple attenuation and velocity model to replicate the observed multi-pathing phenomena. The relative arrival time differences between the direct P-waves

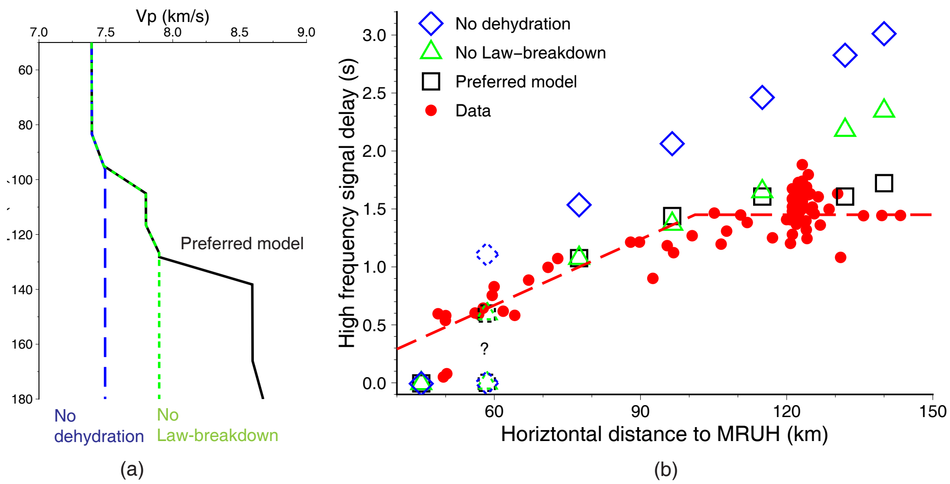

Figure 9: Three Vp models of subducted oceanic crust tested, and time delays of high frequency signals. (a) Three used depth profiles of Vp of the oceanic crust. The black line corresponds to our preferred Vp model, used in Fig. 7. The green dashed line is Vp model without the lawsonite and talc breakdown (corresponding seismograms shown in Fig. S8). The blue dashed line shows Vp model without any dehydration processes (seismograms in Fig. S10). (b) Time delays for modeled and observed high frequency signals. The red solid dots represent the data (Fig. 4d). The red dashed line is the same as that in Fig. 4d. The black squares are from Fig. 7d, corresponding to our preferred model. The blue diamonds are from Fig. S10, and and the green triangles are from Fig. S8. The corresponding Vp models are shown in (a).

and the delayed signals can be explained by a increased Vp in the oceanic crust, which might be associated with the (lawsonite,talc) - eclogite transition. Of course, using a different model of mantle wedge could change the arrivals of both direct P-waves (Fig. S11) and the delayed signals. However, the data can be explained by simple models of velocity and attenuation (Fig. 7) and the derived basalt - eclogite transition is consistent with previous studies (*Kita et al.*, 2006; *Shiina et al.*, 2013).

4. Discussion

The Pacific plate beneath Japan is old, subducting quickly and therefore an archetypical cold slab (*Peacock and Wang*, 1999), so the phase transitions of basalt assemblages might be delayed to greater depths than that in warmer slabs, such as Cascadia and southwest Japan. As a major dehydration reaction, the blueschist - eclogite transition might occur at a depth of $\sim$100 km, much deeper than in warm slabs. This transition gives rise to a 4% Vp increase (Fig. 5b) and turns more than 2 wt % crystallographically bound water into free fluid (Fig. 5a), which may cause elevated pore pressure and therefore promote a higher level of seismicity. Then the buoyant fluid water may migrate up into the mantle wedge and form the serpentinite layer (*Kawakatsu and Watada*, 2007).

The (lawsonite, talc) - eclogite transition in our study region occurs at a greater depth than the blueschist - eclogite transition (Fig. 5a) and has been investigated less due to the reduced level of seismicity at the depths of $>$150 km and the lack of seismic stations in the ocean. Receiver functions (*Kawakatsu and Watada*, 2007) and P-to-S converted waves (*Shiina et al.*, 2013) support the significant increase of Vp in the oceanic crust beneath northeastern Japan at depths of 130 km - 150 km. Our results support a 9% Vp increase at a depth of around 138 km (Fig. 5b), that gives rise to a high velocity oceanic crust at depths greater than 150 km. However, *Abers* (2005) investigated guided waves in various slabs, including under Japan, and proposed an LV oceanic crust at the top of slabs extending to depths greater than 150 km. Moreover, a detailed investigation of guided waves also supports an LV oceanic crust beneath Northern Japan persisting to depths of at least 220 km (*Garth and Rietbrock*, 2014a). The different results from those studies might be due to lateral variations of temperature in the subducting slab, incorrect or incomplete understanding of guided waves and the presence of uncertainties in structural constraints. For example, the guided waves observed by *Garth and Rietbrock* (2014a) only sample the slab beneath Northern Japan. Similarly, most data in *Abers* (2005) sample the slab beneath further North Japan and only a few raypaths travel the shallow (<150 km) portion of the slab beneath central Honshu, northeastern Japan. Indeed, our dataset (Fig. 4c) also indicates a lack of observable guided waves. Thus, an LV oceanic crust at depths greater than 150 km beneath Northern Japan is supported by the investigations of guided waves, but there is no such evidence for the central Honshu. In contrast to Northern Japan, our study indicates a high velocity oceanic crust beneath central Honshu at depths greater than 150 km. This might be due to its warmer temperature and therefore shallower eclogitization than Northern Japan. However, 3D numerical simulations of thermal structure (*Wada et al.*, 2015; *Morishige and van Keken*, 2014) indicate that the slab beneath northern Japan is warmer than that under northeastern Japan. Hence, an alternative possibility could be an overestimation of Vp of the oceanic crust in previous studies of guided waves due to the exaggerated role of LV oceanic crust in dispersion. For example, *Garth and Rietbrock* (2014a) observed dispersed P-waves or guided waves from three intermediate-focus earthquakes beneath northern Japan and attributed them to an LV oceanic crust. However, two of these three earthquakes were investigated by *Furumura and Kennett* (2005), who explained these signals by elongated heterogeneities in the slab. In other words, an LV oceanic crust is not necessary in their model. The presence of such laminar structures has been suggested in other subduction zones (e.g. *Sun et al.*, 2014). Elongated heterogeneities in the slab mantle could originate from melt-rich shear bands or channels when oceanic lithosphere is created at a ridge (*Sun et al.*, 2014; *Holtzman and Kendall*, 2010), though they may not exist in oceanic crust. Thus, further studies of those dispersed signals are needed to distinguish between the roles of elongated heterogeneities and LV oceanic crust.

A 4% Vp increase due to blueschist - eclogite transition and a 9% Vp increase associated with the (lawsonite, talc) - eclogite transition (Fig. 5b) replicates our data. Vp profile in Fig. 5b is calculated from a fully hydrated MORB model. However, the presence of aqueous fluid may affect the velocity of subducted oceanic crust, which is not accounted for here. Estimating pore fluid is critical for understanding the spatial distribution and migration of water in subduction context, but deriving the pore fluid from seismic velocity has large uncertainty, partly due to the complex relationship between seismic velocity and pore geometries (*Takei*, 2002).

In this study, we use simple Qp and Vp models (Fig. 7) to explain the data. Many types of structural complexities in the subduction context are not accounted for here. For example, volumetric heterogeneities are believed to widely exist in the Earth, from the uppermost crust (*Sato et al.*, 2012) to the inner core (*Wu and Irving*, 2017). In particular, strong small-scale heterogeneities beneath the volcanic arc in the Tohoku region have been reported (*Takahashi et al.*, 2009), which are not modeled in the simulations. These small-scale heterogeneities could cause peak delay and broadening of the high frequency seismic wave envelope (*Takahashi et al.*, 2009; *Sato et al.*, 2012). Such heterogeneities may give rise to scattering attenuation in the oceanic crust, which would decrease the delayed high frequency signals. On the other hand, scattering could facilitate the escape of seismic waves in the oceanic crust and could therefore enhance the delayed signals. The details of these heterogeneities in the subduction context, such as velocity perturbations and geometries, are still not fully constrained.

5. Conclusion

As a multi-pathing phenomenon, guided waves have been broadly investigated to prove the presence of subducted LV oceanic crust. Here, we observe another type of multi-pathing from earthquakes with depths greater than $\sim$110 km, in which the broadened direct P-waves are followed by delayed higher frequency P-wave signals. The remarkably different frequencies of the direct P-waves and delayed signals are mainly controlled by attenuation variation and the delay times are affected by the velocity of the oceanic crust. We demonstrate the use of these multi-pathing effects in constraining the structure of the subducted oceanic crust below central Honshu, northeastern Japan. In traditional guided wave scenarios, the oceanic crust has a low velocity and therefore serves as wave guide to trap the seismic waves. In our study, we find that the different frequency content of the direct and delayed signals result from different attenuation in the back-arc mantle and subducted oceanic crust. Distinct from traditional guided waves, the formation of multi-pathing effects here does not require the oceanic crust to have low velocity, though LV oceanic crust may be present at depths less than $\sim$100 km. Furthermore, our observation does not need any particular decoupling mechanism to make the waves escape the oceanic crust. Thus, the multi-pathing effects in this study offer us another tool to image subducted oceanic crust at depths greater than $\sim$100 km, especially where guided waves might not be observable or applicable.

Our SPECFEM2D simulations successfully replicate the multi-pathing effects. The direct P-waves travel through the back-arc mantle wedge with high attenuation and therefore contain less high frequency content than the delayed signals. Relative to the direct P-waves, the arrival times of the delayed signals first increase and then become constant with the horizontal distance. This trend can be explained by a 9% Vp increase in the oceanic crust at a depth of $\sim$138 km and we attribute it to the (lawsonite, talc) - eclogite transition. This Vp increase gives rise to high velocity of subducted oceanic crust at depths greater than 150 km, where seismicity level is reduced significantly. This eclogitization might be also linked with the occurrence of earthquake nests, as proposed by *Nakajima et al.* (2013b).

Traditionally, the use of high frequency seismic waves is impeded by their complex interactions with 3D structure and the expense of numerical simulations. Here, we show that investigating some observable properties, such as the relative travel times, of high frequency body waves, with the help of enhanced computation capability, can advance our understanding of subduction zone structure, although accurately fitting the amplitudes of high frequency waves is still challenging.

6. Acknowledgments

We are grateful for reviews from two anonymous reviewers which helped to improve the manuscript. We thank Jeroen Tromp for his helpful suggestions on the computation of travel time sensitivity kernels. Data have been collected from the NIED Hi-net (http://www.hinet.bosai.go.jp/). We used the earthquake catalog from Japan Meteorological Agency (JMA), as distributed by the International Seismological Centre (http://www.isc.ac.uk/). The authors acknowledge the use of the GMT (*Wessel and Smith*, 1998) and SAC (*Goldstein et al.*, 2003) software packages.

References

Abers, G. A. (2000), Hydrated subducted crust at 100–250 km depth, *Earth Planet. Sci. Lett*, *176*(3-4), 323–330, doi:10.1016/s0012-821x(00)00007-8.

Abers, G. A. (2005), Seismic low-velocity layer at the top of subducting slabs: observations, predictions, and systematics, *Phys. Earth Planet. Inter.*, *149*(1-2), 7–29, doi:10.1016/j.pepi.2004.10.002.

Chen, M., J. Tromp, D. Helmberger, and H. Kanamori (2007), Waveform modeling of the slab beneath Japan, *J. Geophys. Res.*, *112*(B2), B02305, doi:10.1029/2006jb004394.

Connolly, J. (2005), Computation of phase equilibria by linear programming: A tool for geodynamic modeling and its application to subduction zone decarbonation, *Earth Planet. Sci. Lett*, *236*(1-2), 524–541, doi:10.1016/j.epsl.2005.04.033.

Furumura, T., and B. Kennett (2005), Subduction zone guided waves and the heterogeneity structure of the subducted plate: Intensity anomalies in northern Japan, *J. Geophys. Res.*, *110*, B10302, doi:10.1029/2004JB003486.

Garth, T., and A. Rietbrock (2014a), Downdip velocity changes in subducted oceanic crust beneath Northern Japan–insights from guided waves, *Geophys. J. Int.*, *198*(3), 1342–1358, doi:10.1093/gji/ggu206.

Garth, T., and A. Rietbrock (2014b), Order of magnitude increase in subducted H_2O due to hydrated normal faults within the Wadati-Benioff zone, *Geology*, *42*(3), 207–210, doi:10.1130/g34730.1.

Goldstein, P., D. Dodge, M. Firpo, and L. Minner (2003), SAC2000: Signal processing and analysis tools for seismologists and engineers, *The IASPEI International Handbook of Earthquake and Engineering Seismology*, *81*, 1613–1620.

Green, H. W., and P. C. Burnley (1989), A new self-organizing mechanism for deep-focus earthquakes, *Nature*, *341*(6244), 733–737, doi:10.1038/341733a0.

Hacker, B. R. (2008), H_2O subduction beyond arcs, *Geochem. Geophys. Geosyst.*, *9*(3), Q03001, doi:10.1029/2007GC001707.

Hacker, B. R., G. A. Abers, and S. M. Peacock (2003), Subduction factory 1. Theoretical mineralogy, densities, seismic wave speeds, and H_2O contents, *J. Geophys. Res.*, *108*(B1), 2029, doi:10.1029/2001jb001127.

Hobbs, B. E., and A. Ord (1988), Plastic instabilities: Implications for the origin of intermediate and deep focus earthquakes, *J. Geophys. Res.*, *93*(B9), 10,521–10,540, doi:10.1029/jb093ib09p10521.

Holtzman, B. K., and J.-M. Kendall (2010), Organized melt, seismic anisotropy, and plate boundary lubrication, *Geochem. Geophys. Geosyst.*, *11*(12), Q0AB06, doi:10.1029/2010gc003296.

Iwamori, H. (2007), Transportation of H_2O beneath the Japan arcs and its implications for global water circulation, *Chem. Geol.*, *239*(3-4), 182–198, doi:10.1016/j.chemgeo.2006.08.011.

Kawakatsu, H., and S. Watada (2007), Seismic Evidence for Deep-Water Transportation in the Mantle, *Science*, *316*(5830), 1468–1471, doi:10.1126/science.1140855.

Kennett, B. L. N., and T. Furumura (2008), Stochastic waveguide in the lithosphere: Indonesian subduction zone to Australian craton, *Geophys. J. Int.*, *172*(1), 363–382, doi:10.1111/j.1365-246x.2007.03647.x.

Kirby, S., R. E. Engdahl, and R. Denlinger (1996), Intermediate-depth intraslab earthquakes and arc volcanism as physical expressions of crustal and uppermost mantle metamorphism in subducting slabs, in *Subduction top to bottom*, edited by G. E. Bebout, D. W. Scholl, S. H. Kirby, and J. P. Platt, pp. 195–214, American Geophysical Union, doi:10.1029/GM096p0195.

Kita, S., T. Okada, J. Nakajima, T. Matsuzawa, and A. Hasegawa (2006), Existence of a seismic belt in the upper plane of the double seismic zone extending in the along-arc direction at depths of 70–100 km beneath NE Japan, *Geophys. Res. Lett.*, *33*, L24310, doi:10.1029/2006gl028239.

Kobayashi, M., S. Takemura, and K. Yoshimoto (2015), Frequency and distance changes in the apparent P-wave radiation pattern: effects of seismic wave scattering in the crust inferred from dense seismic observations and numerical simulations, *Geophys. J. Int.*, *202*(3), 1895–1907, doi:10.1093/gji/ggv263.

Komatitsch, D., and J. Tromp (1999), Introduction to the spectral element method for three-dimensional seismic wave propagation, *Geophys. J. Int.*, *139*(3), 806–822, doi:10.1046/j.1365-246x.1999.00967.x.

Komatitsch, D., and J.-P. Vilotte (1998), The spectral element method: an efficient tool to simulate the seismic response of 2D and 3D geological structures, *Bull. Seismol. Soc. Am.*, *88*(2), 368–392.

Liu, X., D. Zhao, and S. Li (2014), Seismic attenuation tomography of the Northeast Japan arc: Insight into the 2011 Tohoku earthquake (Mw 9.0) and subduction dynamics, *J. Geophys. Res.*, *119*(2), 1094–1118, doi:10.1002/2013jb010591.

Luo, Y., J. Tromp, B. Denel, and H. Calandra (2013), 3D coupled acoustic-elastic migration with topography and bathymetry based on spectral-element and adjoint methods, *Geophysics*, *78*(4), S193–S202, doi:10.1190/geo2012-0462.1.

Martin, S., A. Rietbrock, C. Haberland, and G. Asch (2003), Guided waves propagating in subducted oceanic crust, *J. Geophys. Res.*, *108*(B11), 2536, doi:10.1029/2003JB002450.

Martin, S., C. Haberland, and A. Rietbrock (2005), Forearc decoupling of guided waves in the Chile-Peru subduction zone, *Geophys. Res. Lett.*, *32*(23), L23309, doi:10.1029/2005gl024183.

Matsubara, M., K. Obara, and K. Kasahara (2008), Three-dimensional P- and S-wave velocity structures beneath the Japan Islands obtained by high-density seismic stations by seismic tomography, *Tectonophysics*, *454*(1), 86–103, doi:10.1016/j.tecto.2008.04.016.

Morishige, M., and P. E. van Keken (2014), Along-arc variation in the 3-D thermal structure around the junction between the Japan and Kurile arcs, *Geochem. Geophys. Geosyst.*, *15*(6), 2225–2240, doi:10.1002/2014gc005394.

Nakajima, J., S. Hada, E. Hayami, N. Uchida, A. Hasegawa, S. Yoshioka, T. Matsuzawa, and N. Umino (2013a), Seismic attenuation beneath northeastern Japan: Constraints on mantle dynamics and arc magmatism, *J. Geophys. Res.*, *118*(11), 5838–5855, doi:10.1002/2013jb010388.

Nakajima, J., N. Uchida, T. Shiina, A. Hasegawa, B. R. Hacker, and S. H. Kirby (2013b), Intermediate-depth earthquakes facilitated by eclogitization-related stresses, *Geology*, *41*(6), 659–662, doi:10.1130/g33796.1.

Obara, K., K. Kasahara, S. Hori, and Y. Okada (2005), A densely distributed high-sensitivity seismograph network in Japan:Hi-net by National Research Institute for Earth Science and Disaster Prevention, *Rev. Sci. Instrum.*, *76*, 021301, doi:10.1063/1.1854197.

Okada, Y., K. Kasahara, S. Hori, K. Obara, S. Sekiguchi, H. Fujiwara, and A. Yamamoto (2004), Recent progress of seismic observation networks in Japan Hi-net, F-net, K-NET and KiK-net, *Earth Planets Space*, *56*(8), xv–xxviii, doi:10.1186/bf03353076.

Pasyanos, M. E., T. G. Masters, G. Laske, and Z. Ma (2014), LITHO1.0: An crust and lithospheric model of the Earth, *J. Geophys. Res.*, *119*(3), 2153–2173, doi:10.1002/2013jb010626.

Peacock, S. M., and K. Wang (1999), Seismic Consequences of Warm Versus Cool Subduction Metamorphism: Examples from Southwest and Northeast Japan, *Science*, *286*(5441), 937–939, doi:10.1126/science.286.5441.937.

Pozgay, S. H., D. A. Wiens, J. A. Conder, H. Shiobara, and H. Sugioka (2009), Seismic attenuation tomography of the Mariana subduction system: Implications for thermal structure, volatile distribution, and slow spreading dynamics, *Geochem. Geophys. Geosyst.*, *10*(4), Q04X05, doi:10.1029/2008gc002313.

Sato, H., M. C. Fehler, and T. Maeda (2012), *Seismic wave propagation and scattering in the heterogeneous Earth*, vol. 496, Springer, doi:10.1007/978-3-540-89623-4.

Shiina, T., J. Nakajima, and T. Matsuzawa (2013), Seismic evidence for high pore pressures in the oceanic crust: Implications for fluid-related embrittlement, *Geophys. Res. Lett.*, *40*(10), 2006–2010, doi:10.1002/grl.50468.

Shiina, T., J. Nakajima, T. Matsuzawa, G. Toyokuni, and S. Kita (2017), Depth variations in seismic velocity in the subducting crust: Evidence for fluid-related embrittlement for intermediate-depth earthquakes, *Geophys. Res. Lett.*, *44*(2), 810–817, doi:10.1002/2016gl071798.

Shiina, T., J. Nakajima, and T. Matsuzawa (2018), P-wave attenuation in the Pacific slab beneath northeastern Japan revealed by the spectral ratio of intraslab earthquakes, *Earth Planet. Sci. Lett*, *489*, 37–48.

Sun, D., M. S. Miller, N. P. Agostinetti, P. D. Asimow, and D. Li (2014), High frequency seismic waves and slab structures beneath Italy, *Earth Planet. Sci. Lett*, *391*, 212–223, doi:10.1016/j.epsl.2014.01.034.

Syracuse, E. M., P. E. van Keken, and G. A. Abers (2010), The global range of subduction zone thermal models, *Phys. Earth Planet. Inter.*, *183*(1-2), 73–90, doi:10.1016/j.pepi.2010.02.004.

Takahashi, T., H. Sato, T. Nishimura, and K. Obara (2009), Tomographic inversion of the peak delay times to reveal random velocity fluctuations in the lithosphere: method and application to northeastern Japan, *Geophys. J. Int.*, *178*(3), 1437–1455, doi:10.1111/j.1365-246x.2009.04227.x.

Takei, Y. (2002), Effect of pore geometry on Vp/Vs: From equilibrium geometry to crack, *J. Geophys. Res.*, *107*(B2), 2043, doi:10.1029/2001jb000522.

Takemura, S., K. Yoshimoto, and T. Tonegawa (2015a), Velocity increase in the uppermost oceanic crust of subducting Philippine Sea plate beneath the Kanto region due to dehydration inferred from high-frequency trapped P waves, *Earth Planets Space*, *67*(1), doi:10.1186/s40623-015-0210-6.

Takemura, S., K. Yoshimoto, and T. Tonegawa (2015b), Scattering of trapped P and S waves in the hydrated subducting crust of the Philippine Sea plate at shallow depths beneath the Kanto region, Japan, *Geophys. J. Int.*, *203*(3), 2261–2276, doi:10.1093/gji/ggv423.

Tromp, J., C. Tape, and Q. Liu (2005), Seismic tomography, adjoint methods, time reversal and banana-doughnut kernels, *Geophys. J. Int.*, *160*(1), 195–216, doi:10.1111/j.1365-246x.2004.02453.x.

Ueno, H., S. Hatakeyama, T. Aketagawa, J. Funasaki, and N. Hamada (2002), Improvement of hypocenter determination procedures in the Japan Meteorological Agency, *Q. J. Seismol.*, *65*, 123–134.

Wada, I., J. He, A. Hasegawa, and J. Nakajima (2015), Mantle wedge flow pattern and thermal structure in Northeast Japan: Effects of oblique subduction and 3-D slab geometry, *Earth Planet. Sci. Lett*, *426*, 76–88, doi:10.1016/j.epsl.2015.06.021.

Wessel, P., and W. H. Smith (1998), New, improved version of Generic Mapping Tools released, *EOS Trans. Amer. Geophys. Union*, *79*(47), 579–579, doi:10.1029/98EO00426.

Wu, W., and J. C. Irving (2017), Using PKiKP coda to study heterogeneity in the top layer of the inner core's western hemisphere, *Geophys. J. Int.*, *209*(2), 672–687, doi:10.1093/gji/ggx047.

Zhao, D., T. Matsuzawa, and A. Hasegawa (1997), Morphology of the subducting slab boundary in the northeastern Japan arc, *Phys. Earth Planet. Inter.*, *102*(1-2), 89–104, doi:10.1016/s0031-9201(96)03258-x.